Cronfa - Swansea University Open Access Repository

_____

This is an author produced version of a paper published in:
Nanoscale

_____

Cronfa URL for this paper:
http://cronfa.swan.ac.uk/Record/cronfa45492

_____

Paper:

_____

http://www.swansea.ac.uk/library/researchsupport/ris-support/

Nanoscale

ARTICLE

Aqueous electromigration of single-walled carbon nanotubes and co-electromigration with copper ions

Pavan M. V. Raja,[a] Gibran L. Esquenazi,[a] Kourtney D. Wright,[a] Cathren E. Gowenlock,[b] Bruce E. Brinson,[a,c] Shirin Alexander,[b] Daniel R. Jones,[b] Varun Shenoy Gangoli,[a,c] and Andrew R. Barron*[a,b,d]

The electromigration behaviour of raw and acid purified single walled carbon nanotubes (SWCNTs) in dilute aqueous systems (0.0034 mg/mL), in the absence of surfactant, with the addition of either 0.85 M acetic acid or 0.1 M $CuSO_4$, was evaluated using a 2-inch copper cathode and either a 2-inch copper or 0.5-inch platinum anode. The results showed that the electromigration of raw SWCNTs (with a high catalyst residue) in the presence of $CuSO_4$ resulted in the formation of a Cu-SWCNT composite material at the cathode. In contrast, acid purified SWCNTs were observed to diffuse to a copper anode, creating fibrils agglomerates with "rice-grain"-like morphologies. Upon acidification with acetic acid (or addition of $CuSO_4$) the direction of electromigration reversed towards the cathode as a result of coordination of Cu^{2+} to the functional groups on the SWCNT overcoming the inherent negative charge of the acid purified SWCNTs. The result was the co-deposition of SWCNTs and Cu metal on the cathode. Addition of 0.005 M EDTA sequesters some of the Cu^{2+} and resulted in the separation of metal decorated SWCNTs to the cathode and un-decorated SWCNTs to the anode. The resulting SWCNT and Cu/SWCNT deposits were characterized by Raman spectroscopy, XPS, SEM, EDS, and TEM.

Introduction

One of the applications proposed for carbon nanotubes (CNTs) is as highly electrically conducting, high-ampacity cables for the more efficient (low loss) transport of electricity as compared to the traditionally used copper wires.[1,2] Prior research has shown that electrons are capable of ballistic transport through the inner diameter of single walled carbon nanotubes (SWCNTs) with armchair chirality,[3] and could be used as a superior substitute for copper wires.[1,4] Despite promise, the realization of SWCNT-based transmission cables has significant technical challenges to be overcome. One near term solution proposed as a stopgap involves the improvement in conductivity and ampacity of copper by the addition of CNTs.[5,6] The best results to date show a conductivity of 4.7×10^5 S/cm and an ampacity of 630×10^6 A/cm^2, which is a 100-fold increase in the ampacity of the Cu-CNT composite versus Cu.[7]

The fabrication of the Cu-CNT composite material, termed ultra-conductive copper, has been accomplished in a variety of different ways including electrolytic co-deposition,[8,9] powder metallurgy,[10] and electroless plating.[11,12] Of these the electrolytic co-deposition is of interest since the composition of the resulting films may potentially be controlled through the solution composition and process conditions. In prior work, MWCNTs were employed in an acid bath (0.55 M H_2SO_4) with a poly(acrylic acid) dispersant.[9] It would be of interest to be able to perform similar co-deposition at lower acidity (neutral pH) and, most importantly, without a dispersant that adds potential impurities in the resulting Cu-CNT composite.

A systematic analysis of electromigration of nanomaterials is important for promoting: better metal-nanomaterial composites for applications such as improved electrical conductors; better electroplated multifunctional composite coatings; better understanding of how electrochemical processes can be reversed with the goal of material purification/separations, and/or recycling.

CNTs have previously been reported as being suitable electrodes for electrophoresis,[13,14] but studies where they are part of the mobile phase are limited. CNTs have been deposited onto selected substrates by electrophoresis deposition,[15,16] and a/c electrophoresis has been employed for the orientation of CNTs,[17] the production of devices,[18,19] and separation in the vapour phase.[20]

Herein we report the electromigration behaviour of raw and acid purified SWCNTs in aqueous systems in the absence of dispersant agents, and investigated the dependence on functionalization and metal coordination for migration to the cathode or anode. The goals of the study include: understand the mechanism of migration of nanomaterials between

a. Department of Chemistry, Rice University, Houston, TX 77005, USA. E-mail: arb@rice.edu

b. Energy Safety Research Institute, Swansea University Bay Campus, Swansea, SA1 8EN, UK. a.r.barron@swansea.ac.uk

c. Smalley-Curl nanoCarbon Center, Rice University , Houston, Texas 77005, USA.

d. Department of Materials Science and Nanoengineering, Rice University, Houston, Texas 77005, USA

electrodes under an applied DC electric field; to analyse how bath composition and processing of nanomaterials can impact migration of the nanomaterials to the electrode surfaces; and to evaluate co-electrodeposition mechanisms involving nanomaterials and metal species.

Experimental

Materials and Methods

All reagents were purchased from Sigma Aldrich Ltd. and used as received unless otherwise noted. Raw HiPco SWCNTs (09-HiPco-0093, batch No. 188.4) were obtained from the Carbon Nanotube Laboratory (CNL) at Rice University.

Acid-treated and base-neutralized purified SWCNTs (a-SWCNTs) were prepared by a modification of a previously reported procedure.[21] Raw SWCNTs (15 mg) were subjected to a 5-second microwave treatment followed by refluxing in a 3:1 mixture of H_2SO_4 and HNO_3 (80 mL, prepared by the dilution of 40 mL of a 50:50 mixture of the concentrated acid mixture with 40 mL DI water) for 4 hours. The dispersion was diluted with excess DI water and filtered through a 0.1 µm PVDF membrane (Millipore Durapore, 47mm diameter) under vacuum. The filter cake was washed with copious amounts of DI water to remove residual acid, and neutralized with the addition of NH_4OH solution. The filter cake was then washed with an excess amount of DI water till the pH of the water above the filter cake was close to 7.0 (as measured by a pH paper) and the reddish hue of the filtrate was no longer present. Finally, the filter cake was washed with excess acetone to remove the majority of the water. The almost-dry filter cake was weighed along with the filter membrane of a known tared weight (to determine % yield) and immediately transferred to a 20 mL scintillation vial. DI water (16 mL) was added to the vial, which was capped and manually shaken to dislodge the filter cake from the membrane and suspend into the water. The PTFE membrane was then removed and discarded, and the contents of the vial were sonicated for 10 minutes till a uniform and stable black aqueous dispersion was obtained. A 16 mL batch of purified SWCNT aqueous dispersion with a final concentration of ~0.34 mg/mL was obtained (yield ≈ 36%) in this manner, which was used for the electromigration experiments, see below.

In order to better understand the fundamental interactions (e.g., adsorption/desorption) between CNTs and copper ions (especially at defect sites and functional groups on nanotube surfaces) a control experiment was conducted: acid-treated SWNTs (0.34 mg), $CuSO_4.5H_2O$ (10.4 mg) with or without ethylenediaminetetraacetic acid (EDTA, 10.0 mg) were sonicated in DI water (1 mL) for 10 mins, then filtered under vacuum onto a polycarbonate filter membrane. The SWNTs were washed 3 times with DI water and re-suspended in DI water by sonication.

Morphologies of samples were analysed using FE-SEM (FEI Quanta 400). SEM samples were prepared on carbon tape mounted on aluminium SEM stubs. Transmission electron microscopy (TEM) images were recorded using a Jeol 1230 High Contrast TEM with a W filament and an operating voltage of 80 kV or using a Jeol 2100 TEM with a field emission electron gun and an operating voltage of 200 kV. TEM samples were prepared by drop-drying a dilute solution of carbon nanotubes suspended in EtOH onto a 300-mesh gold grid with a lacy carbon film (Agar-Scientific Ltd). Chemical/compositional analyses were carried out using EDS (FEI Quanta 400 or Hitachi TM3030 Plus SEM). X-ray photoelectron spectra (XPS) were recorded on either a PHI Quantera XPS Scanning Microprobe or a Kratos Axis Supra instrument, using monochromated Al-K_α X-ray sources (1486.7 eV). All spectra were recorded using a charge neutralizer to limit differential charging and subsequently calibrated to the carbon peak at a binding energy of 284.5 eV. Survey scans were recorded at a pass energy of 140 eV and high-resolution data at a pass energy of 26 eV. Data was fitted using MultiPak software.

TGA (SDT Q-600 model, TA Instruments) was carried out under air. UV-visible spectrophotometry was collected using a Shimadzu UV3101PC spectrophotometer. Charge analysis of the nanotubes in dispersion was conducted using the Malvern Zetasizer ZN Nanoseries Zeta Potential Analyzer. Raman spectra were recorded on a Renishaw InVia confocal Raman spectrometer with the exciting wavelength at 532 nm and a 50x objective lens.

Electrolysis

Electroplating was performed using a Variable Regulated Power Supply (Model XP-85) setup from Elenco Precision, Inc., at a setting of 14.4 V DC. The electrolysis of acid-treated SWCNTs (a-SWCNTs) or nanotube-free controls was performed in a 20-mL scintillation vial as the plating bath, which allowed a solution volume of 10-12 mL. In the case of raw SWCNTs, a 150 mL plating bath was used to enable dynamic dispersion using a magnetic stir bar (1000-1200 rpm). The copper electrodes

Table 1. Experimental conditions chosen for electroplating/electromigration studies using copper ions

Experiment	Cathode	Anode	SWCNTs (0.0034 mg/mL)	Acetic acid (mol/dm³)	$CuSO_4$ (mol/dm³)	EDTA (mol/ dm³)
1	Cu	Cu	-	-	-	-
2	Cu	Pt, Cu	Raw	-	-	-
3	Cu	Cu	Raw	-	0.1	-
4	Cu	Cu	a-SWCNT	-	-	-
5	Cu	Pt, Cu	a-SWCNT	0.85	-	-
6	Cu	Cu	a-SWCNT	-	0.1	-
7	Cu	Cu	a-SWCNT	0.85	-	0.005

Nanoscale **Paper**

were typically ~2″ long while the platinum anode (when used) was 0.5″ in length. The electrodes were spaced 5 mm apart.

A range of experiments were conducted during this study to address the following research scenarios: (1) migration of raw and purified SWCNTs toward electrodes in the plating bath, (2) effect of electrode materials, (3) effect of the plating process on the electrode surfaces, (4) fundamental mechanics of co-migration of nanotubes and copper ions toward an electrode, (5) effect of various additives such as chelating agents (e.g., disodium EDTA to evaluate if selective partitioning of CNTs is possible, suspended copper particles, and pH modifiers. Table 1 summarizes the various experimental conditions pertaining to the electroplating experiments.

Results and discussion

Raw HiPco SWCNTs

The extreme hydrophobic nature of raw HiPco SWCNTs is demonstrated by a measured water contact angle of 129±2° for a film deposited on glass (Fig. S1, see ESI). The hydrophobicity means they show poor miscibility in DI water despite attempts to sonicate them extensively for over an hour.[22] Further sonication would likely have modified their structure due to the introduction of defect sites and/or resulted in cutting.[23] The hydrophobicity of the raw nanotubes has implications in terms of the physical forces needed to keep them dispersed in an electroplating apparatus.

In order to maintain dispersion, the raw SWCNTs needed to be continually vortexed (400-1300 rpm) within the aqueous electroplating bath, using a magnetic stir bar. Applying a voltage of 14.4 V to the stirring aqueous suspension and using an anode (either platinum or copper) and a copper wire cathode resulted in the formation of hydrophobic clumps of SWCNTs suspended in the vortexed bath. Enhanced dispersion is possible when the raw SWCNTs were sonicated in DMF (0.2 mg/mL); subsequent electrolysis (14.4 V) resulted in the partition of the SWCNTs between the platinum wire anode and copper wire cathode (Fig. S2, see ESI).

Similar results were observed when hydrophobic nanotube clumps were vortexed between a copper anode and a copper cathode. In this case, while the nanotubes were poorly dispersed in DI water (Fig. S3, see ESI), they were observed again to partition between the two electrodes, with some clumps of the nanomaterial still floating at the meniscus of the

Fig. 1. Photographs of raw SWCNTs after 102 seconds electrolysis in DI water. The left electrode is the anode while the right electrode is the cathode.

bath (Fig. 1). The deposits on either electrode were mostly non-adherent and could be easily wiped off. A few SWCNTs adhered more persistently if the cathode surface was made of copper mesh (instead of wire); however, this appears to be due to physical entrapment of the nanotubes on the mesh.

The partitioning of the raw SWCNTs to both cathode and anode suggest a portion of the SWCNTs exhibit a positive charge making them attractive to the cathode, while others have an overall negative charge resulting in aggregation to the anode. The Raman spectrum of the raw SWCNTs (Fig. 2) shows a low I_D/I_G ratio (0.151 ±0.003) indicative of a low level of sidewall functionalization. Such functionality has been shown to comprise of oxygen functional groups such as hydroxides, carboxylic acids and epoxides.[24,25] These types of substituents would result in a negative charge centres in aqueous suspension; however, TGA indicates that in addition to side wall functionalization there is significant oxidized iron catalyst present, which may vary from 20-40% within a single batch.[26-28] TEM images of the raw HiPco SWCNTs (Fig. S4a, see ESI) show particles that are consistent with the presence of catalyst residue.
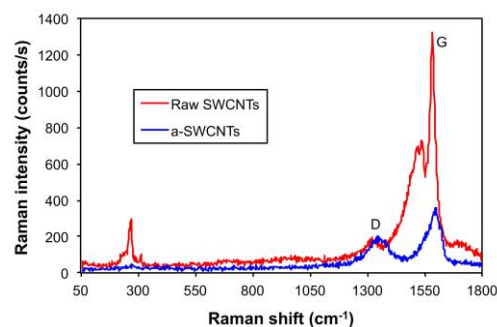

Fig. 2. Raman spectra of raw SWCNTs and a-SWCNTs.

Based upon the aforementioned we propose that the observed migration to cathode of raw-SWCNTs is likely to be due to the catalyst residue (FeO_x from XPS) dragging along the attached nanotube bundles.[29] Further support for this mechanism is provided by the report by Jones et al., that nano-iron is readily transported through electrophoresis.[30] In contrast, anodic migration could have been caused by some fraction of the raw-SWCNTs having a large number of native oxygen defect sites, and presumably a lower catalyst content as well. The partitioning between cathode and anode is presumably due to inhomogeneous distribution of catalyst residue and/or the sidewall functional groups. The inhomogeneity of catalyst in SWCNTs samples has been previously reported as contributing to inhomogeneous functionalization via the Billups-Birch reaction.[28] Applying a voltage of 14.4 V to the stirring suspension of raw SWCNTs in a $CuSO_4$ solution (0.1 mol/dm³) using a copper anode and a copper cathode resulted in the co-migration of the SWCNTs with copper ions to form a loosely bound deposit exclusively on the cathode (Fig. 3).[9] In addition, the blue colour of the Cu^{2+} solution decreases with time suggesting electrodeposition on the cathode of Cu from solution.
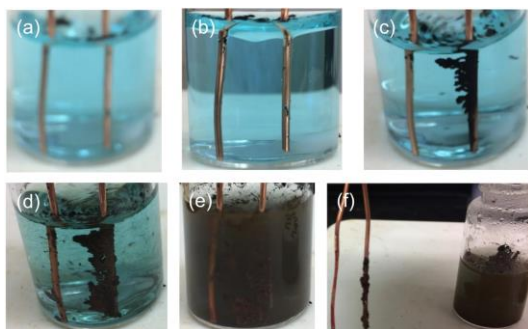
Fig. 3. Photographs of raw SWCNTs during electrolysis in the presence of Cu^{2+} ions at time intervals: (a) 0 s, (b) 16 s, (c) 40 s, (d) 160 s, (e) 305 s, and (f) 446 s. The migration to the cathode (right hand electrode) and co-electrodeposition of Cu from solution as indicated by the loss of the blue colour from the solution.

Fig. 4. SEM images of the cathode after electrolysis of raw SWCNTs in the presence of Cu^{2+} ions. Scale bar = 10 μm.

It is well known that Cu^{2+} ions are readily adsorbed onto SWCNTs[31] and epoxide functionalized MWCNTs.[32] Coupling this observation with the known presence of epoxide (and other oxygen ligand substituents) on raw-SWCNTs,[24] suggests that the Cu^{2+} adsorbs to the surface of the raw-SWCNTs overcoming the negative charge of those nanotubes that would have otherwise migrated to the anode, and ensuring all of the nanotubes exhibit an 'effective positive charge' and hence migrate to the cathode.

As seen in Fig. 3f, when the electrode was removed from the solution the deposit adhered more strongly than in the absence of added Cu^{2+} ions. An SEM image of the cathode (Fig. 4) shows the adhered material to be a combination of nanotubes and 0.5-8.0 μm particles. Based upon EDS (Cu = 83.97 at%, O = 3.45 at%) the latter is likely Cu with some oxide. We propose that the large Cu/CuO aggregates are a combination of electro deposition of Cu^{2+} from solution directly to the electrode surface and deposition seeded by the functionality of the nanotubes.[12] We also note that SEM images of the anode show some particulate deposits (Fig. S5, see ESI); however, this appears to be material transferred from the cathode by the vortexing since the quantity is low and poorly adhered. More importantly, there appears to be little change in the morphology of the anode suggesting that the deposited Cu is primarily from the Cu^{2+} in solution and not transfer from anode to cathode. While the presence of oxide may not necessarily be a positive development in the context of electrical applications, optimization of its presence can potentially enable applications such as the fabrication of better sensors to accurately detect the presence pharmaceutical products in the bloodstream.[33]

Although the electro deposition of Cu (with subsequent partial oxidation) is expected from a $CuSO_4$ solution, deposition is also expected from copper anode to the cathode in the absence any soluble Cu^{2+}. Migration of copper ions from anode to cathode was verified through a control experiment where two copper electrodes were subjected to a 14.4V direct current potential difference in a plating bath comprising of only DI water. The reaction is significantly slower than for raw-SWCNTs and $CuSO_4$, but does result in gradual blue coloration in the vicinity of the electrodes followed subsequently by the
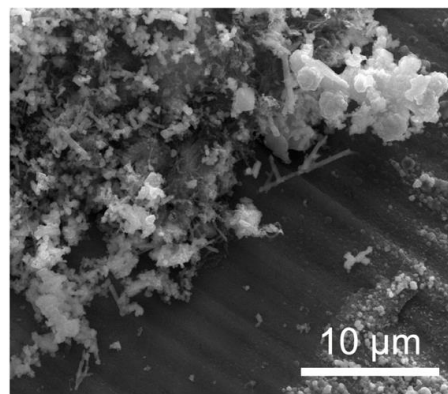
formation of an aggregated material between the electrodes (Fig. S6, see ESI).

SEM analysis (Fig. S7, see ESI) of anode, cathode, and precipitate revealed the anode to be covered with large granular deposits, while the cathode surface looked clean implying that it was predominantly unchanged. Lower magnification images of anode show some degree of pitting, but these pits were covered up with the granular particles, presumably due to non-specific attachment of particles from the bath onto the roughened anode surface. The aggregate comprised of nanoscale particles, mostly composed of Cu and CuO as determined by EDS analysis (C 3.27 ±1.79 at%, O 0.60 ±0.34 at%, and Cu 96.33 ±2.1 at%). These results confirm our proposal that the deposit on the cathode upon electrolysis of raw-SWCNTs/Cu^{2+} is not due to electrode to electrode transfer, but rather the migration of SWCNT-$(Cu^{2+})_n$ complexes to the cathode surface and seeding of Cu growth on those complexes.

Acid Purified SWCNTs

In order to remove any effect of the high catalyst residue content, the SWCNTs were purified using an acid treatment followed by base neutralization (see Experimental). This process has previously been employed to provide low catalyst residue samples;[26] however, caution should be employed since the CNTs dissolved completely when refluxed in the concentrated acid mixture.

The TEM of acid treated SWCNTs (a-SWCNTs) shows a dramatic reduction in catalyst residue particles as compared to the raw SWCNTs (Fig. S4, see ESI). TGA of the a-SWCNTs confirms a low catalyst residue content (1.2 wt.%), but it also indicates significant sidewall functionalization.[34] Raman spectroscopy confirms the presence of sidewall functionalization by an increased I_D/I_G ratio (0.55 ±0.03) as compared to the raw-SWCNTs (Fig. 2). The functional groups result in the a-SWCNTs being hydrophilic, as indicated by a low water contact angle of 33.3±2.8° (Fig. S1, see ESI). XPS showed that the Fe content of the raw SWNTs was reduced by the acid treatment.[26] Additionally, the C:O ratio decreased after acid treatment, which is consistent with carboxylation of the SWCNTs.

Acid purified-and-neutralized SWCNTs (a-SWCNTs) are more soluble that raw-SWCNTs and can be suspended readily in DI-water. Applying a voltage of 14.4 V to the un-stirred suspension of a-SWCNTs in aqueous solution using a copper anode and cathode (Table 1) resulted in the migration of the a-SWCNTs to form a loosely bound highly branched deposit on the anode (Fig. 5). Given the presence of carboxylate and hydroxyl functional groups after acid treatment,[27,35] this migration is consistent with them having an overall negative charge. The overall charge is confirmed from Zeta potential measurements (Fig. 6), which show them to have a constant ζ potential value over a wide pH range of 4-10 consistent with good stability in water, at pH < 4 the ζ potential rises.[36]
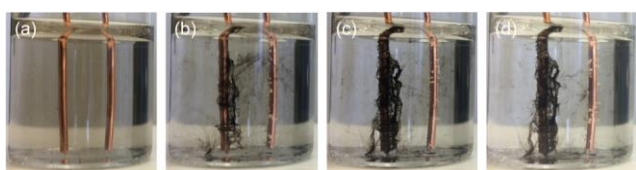

Fig. 5. Images of a-SWCNT migration to the anode upon application of 14.4 V in DI water at time intervals: (a) 0 s, (b) 312 s, (c) 799 s, and (d) 1050s. The left electrode is the anode while the right electrode is the cathode.
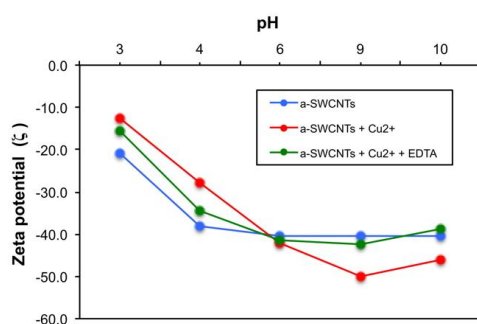

Fig. 6. Zeta potential as a function of pH for (a) a-SWCNTs, (b) a-SWCNTs in the presence of Cu^{2+} ions, and (c) a-SWCNTs in the presence of Cu^{2+} ions after the addition of EDTA.

The large aggregate was easily detached from the anode when it was lifted from the bath, indicating a purely physical interaction with the anode. As such the SEM analysis revealed very few nanotubes on the anode surface (Fig. S8, see ESI) confirming the weak interaction between the electrode and the a-SWCNT aggregates. Surprisingly, while the cathode appeared visually unchanged, the SEM images (Fig. 7) showed the cathode surface to have a uniform layer of the SWCNTs. The cathodic layer is likely due the presence of residual iron catalyst particles that were attracted toward the cathode under the applied electric field. A TEM image of the bundles that detached from the anode is shown in Fig. 8, and show these fibrils are comprised of smaller aggregates of the nanotubes shortened during the acid-treatment purification process such that they coalesced into rice grain-shaped morphologies. The formation of a porous SWCNT network structure on the anode suggests that there is a statistical probability of a SWCNT in solution being attracted to a fresh anode surface or a SWCNT already bound to the surface. The

observation that a small fraction of a-SWCNTs that migrated to the cathode, suggests that electrolysis could be a way to further purify SWCNTs. Further investigation is needed to optimize the phenomenon of cathodic migration of acid-treated SWCNTs as a means of further increasing the their purity.
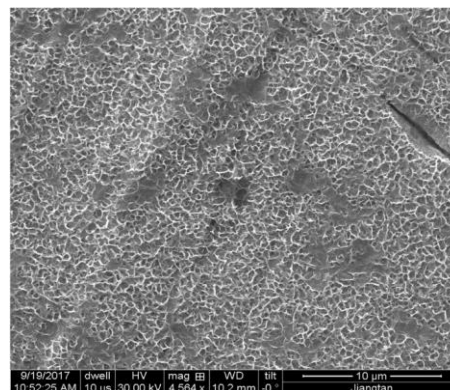

Fig. 7. SEM of the cathode surface after anodic migration of a-SWCNTs. Scale bar = 10 µm.
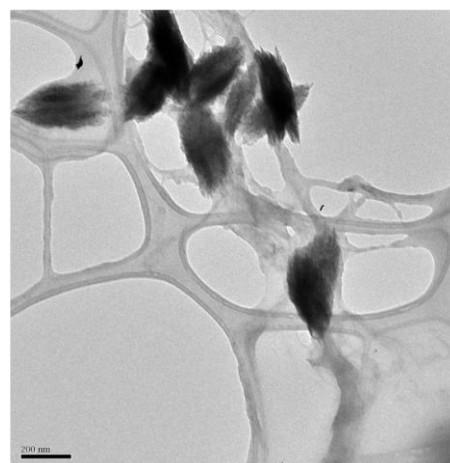

Fig. 8. TEM of the loosely bound deposits that are formed around the anode, which are easily dislodged and re-suspended when electrodes were taken out of the bath and subsequently deposited on the lacy carbon TEM grid. Scale bar = 200 nm.

As with the raw-SWCNTs, any inherent negative charge on the a-SWCNTs should be possible to overcome by coordination with Cu^{2+}, resulting in exclusive migration to the cathode instead of the anode. EDS analysis of a-SWCNTs reacted with $CuSO_4$ in aqueous solution revealed that the nanotubes adsorbed up to 2.6 at% of the Cu^{2+} in solution. This is in good agreement with our recent report that Piranha-etched SWCNTs uptake 14.2 mg Cu/g SWCNT as measured by UV-visible adsorption of the supernatant, which correlates to ca. 2.7 at.%.[12] Electrolysis of a-SWCNTs in the presence of $CuSO_4$ (Table 1) did indeed result in deposition on the cathode (Fig. 9, and Fig. S9 in ESI). The SEM of the anode (Fig. 10a) shows evidence of pitting associated with dissolution of the copper, while the cathode (Fig. 10b) shows the formation of a nanotube rich composite. The appearance of plate-like structures on the anode surfaces in Fig. 10a could have been

due to the deposition of salts on the anode surface despite the precautions in sample preparation undertaken prior to SEM (i.e., washing thoroughly in DI water and drying), EDS analysis of the anode indicates S content (~5 at.%) that supports the presence of salts on the anode surface.
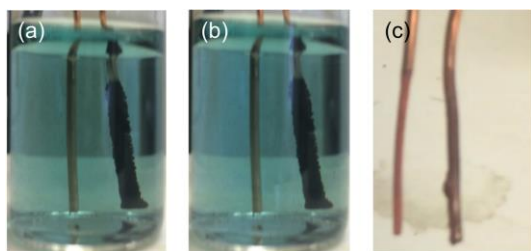

Fig. 9. Photographs of an experiment involving copper electrodes in with a-SWCNTs (0.0034 mg/mL) in a CuSO$_4$ solution (0.1 mol/dm^3) before and after two time intervals of electrolysis: (a) 0 s, (b) 53 s, and (c) 879 s. The left electrode is the anode while the right electrode is the cathode.
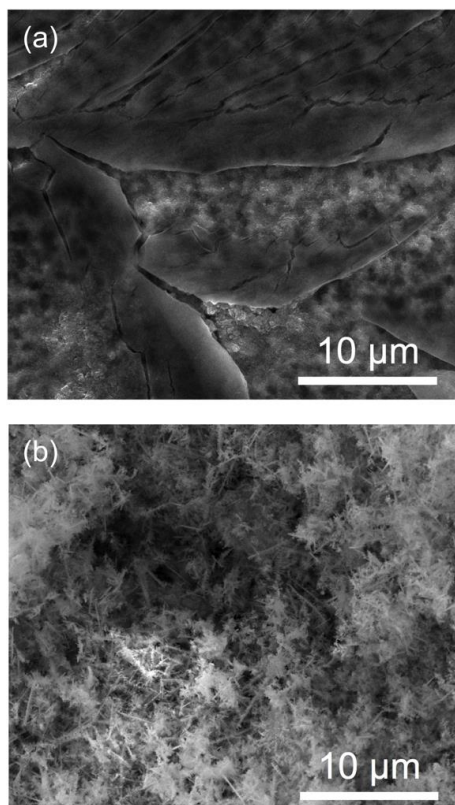

Fig. 10. SEM images of (a) copper anode and (b) copper cathode surfaces after electrolysis of a suspension of a-SWCNTs (0.0034 mg/mL) in a solution of CuSO$_4$ (0.1 mol/dm^3). Scale bars = 10 μm.

If the reversal of migration direction from anode to cathode is associated with the complexation of Cu^{2+} cations to the oxygen functionality of the a-SWCNTs, then a similar effect should be observed with the protonation of sidewall functional groups. Thus, the addition of acetic acid rather than CuSO$_4$ was investigated (Table 1). Under the applied voltage the a-SWCNTs did migrate to the cathode, however, copper was also liberated from the anode and the subsequent deposit comprised a Cu-SWCNT composite, rather than a-SWCNTs

alone. As may be seen in Fig. 11 a blue colour to the solution was produced after 15-30 s. The blue colour intensified with time and the resulting deposit on the cathode was similar in appearance to the result from the electrolysis of a-SWCNTs in CuSO$_4$ solution (Fig. 9).
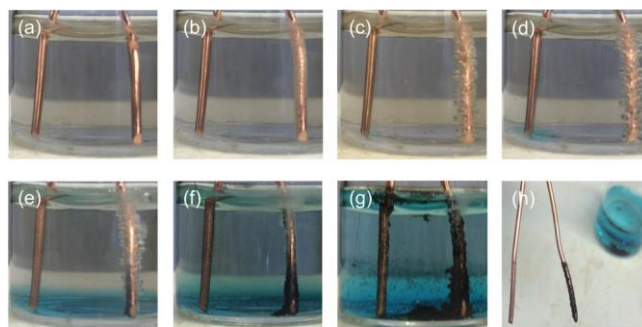

Fig. 11. Photographs of an experiment involving copper electrodes with a-SWCNTs (0.0034 mg.mL) in an acetic acid solution (0.85 mol/dm^3) before and after various time intervals of electrolysis: (a) 0 s, (b) 3 s, (c) 15 s, (d) 30 s, (e) 237 s, (f) 741 s, (g) 1935 s, and (h) 2676 s. The left electrode is the anode and the right electrode is the cathode.

SEM analysis of the electrodes after electrolysis (Fig. 12) revealed a highly pitted anode surface due to erosion. In addition granular particles were also seen likely due to non-specific interactions between the particles formed by the erosion of the anode, dispersed nanotubes, and the anode itself. This is confirmed by EDS analysis that shows comparable
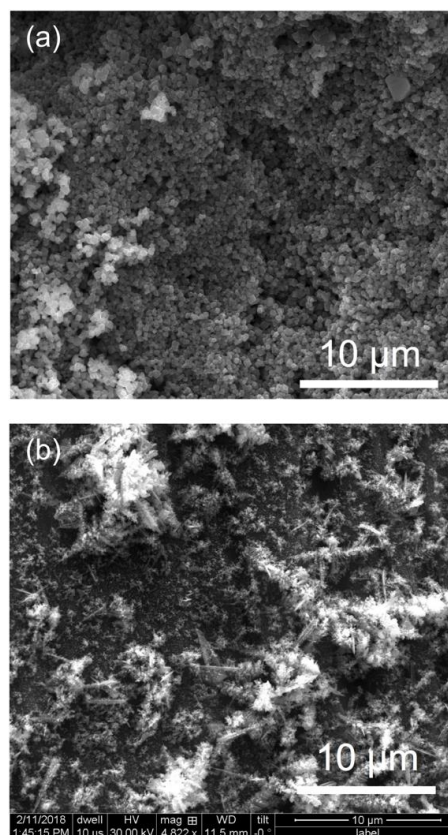

Fig. 12. SEM images of copper (a) anode and (b) cathode surfaces after electrolysis of a suspension of a-SWCNTs (0.0034 mg/mL) in a solution of acetic acid (0.85 mol/dm^3). Scale bars = 10 μm.
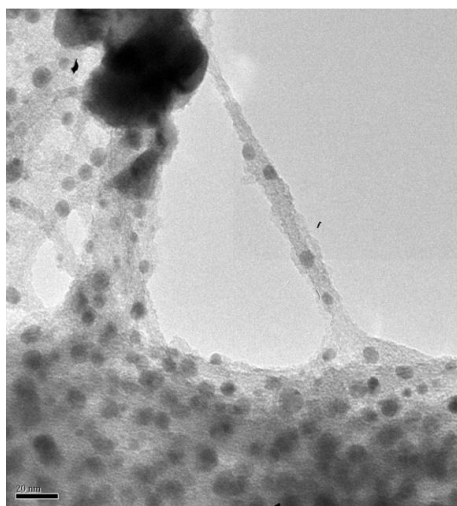
Nanoscale

Fig. 13. TEM images of electroplated cathode deposit formed after electrolysis of a suspension of a-SWCNTs (0.0034 mg.mL) in a solution of acetic acid (0.85 mol/dm³). Scale bar = 20 nm.

Fig. 14. Photographs of an experiment involving copper electrodes with an acetic acid solution (0.85 mol/dm³) before and after various time intervals of electrolysis: (a) 0 s, (b) 5 s, (c) 38 s, (d) 295 s, and (e) 1221 s. The left electrode is the anode while the right electrode is the cathode. Blue coloration is seen 38 seconds onwards suggesting electrode exchange of copper ions migrating from anode to cathode that is eventually results in a brownish-black deposit at the cathode.

carbon content for both anode (~6.1 at.%) and cathode (~5.7 at.%), though the nanotubes were not visible in the case of the anode. In contrast, the cathode shows a nanotube/particle composite morphology. TEM analysis (Fig. 13) of the cathode deposit revealed nanotubes decorated with 10-20 nm sized particles on their surfaces. The decorated nanotube surfaces looked similar to those of Cu seeds formed on the surface of functionalized SWCNTs via electroless deposition.[27] The distribution of carbon almost equally between anode and cathode suggests partitioning of CNTs between the two electrodes though visually the carbon content was more apparent around the cathode (Fig. 12b). The carbon content at the anode could have also likely been due to the presence of adventitious non-CNT carbon.

We propose that the blue solution seen in Fig. 11 is due to the formation of soluble copper salts, presumably $Cu_2(OAc)_4$, through oxidative dissolution of the copper anode (see below). We have shown that $Cu_2(OAc)_4$ coordinates to functionalized SWCNTs and other nanoparticles. Transport of the a-SWCNT-$Cu_2(OAc)_4$ conjugate to the cathode surface provides the reducing environment for the seeding of Cu nanoparticles on the electrode surface (Fig. 13).

In order to confirm the Cu deposited on the cathode is from the oxidative dissolution of the anode and the presence of a-SWCNTs in solution and on the cathode surface is an important factor in the morphology observed; a control experiment was performed with the electrolysis of an acetic acid solution in the absence of a-SWCNTs. As may be seen from Fig. 14 this visually showed the development of blue colour at 38 seconds. From a comparison of the UV-visible spectrum of the electrolysis bath solution, with the spectrum for $Cu_2(OAc)_4$ (Fig. S10, see ESI) is consistent with the in-situ formation of latter in the former reaction.

SEM analysis (Fig. S11, see ESI) of the electrode surfaces shown in Fig. 14 showed pitting on the anode surface and particulate deposits on the cathode surface, which from EDS
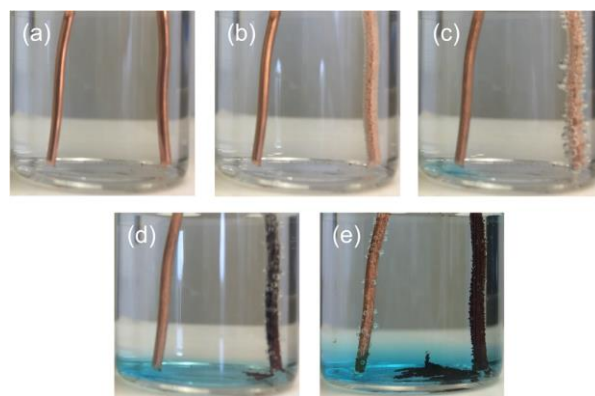
analysis suggests a mixture of Cu and CuO. However, a comparison with Fig. 12b shows the importance of the a-SWCNTs in defining the morphology of the resulting deposited material.

If the electro migration of a-SWCNTs to the anode is reversed by the addition of soluble Cu^{2+} species (either directly or via the dissolution of the Cu anode by addition of acetic acid), then this should be overcome by either competitive complexation of the Cu^{2+} or neutralization of the acetic acid.

When NH_4OH solution (0.5 mL) was added to the electrolysis solution of a-SWCNTs (0.0034 mg/mL) in an acetic acid solution (0.85 M) using copper electrodes, the migration was not reversed. Instead, migration toward the cathode continued, and the resulting deposit on the cathode (Fig. 15) consist of larger Cu particles (20-40 nm) than without NH_4OH addition (5-10 nm, Fig. 13). The increase in particle size could be due to the NH_4OH functioning as an electrolyte, increasing the electrical conductivity of the plating bath. In addition, zeta
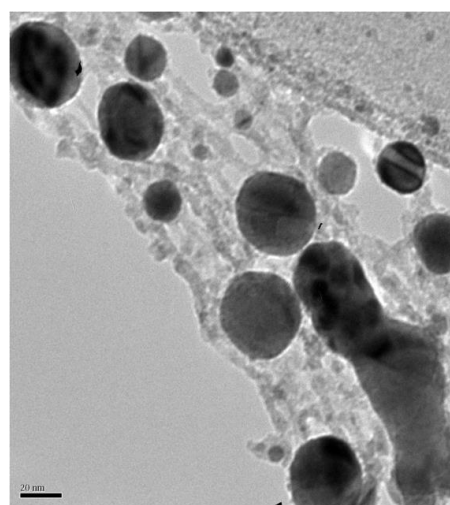

Fig. 14. TEM of electroplated cathode deposit synthesized by electrolysis in a bath containing a-SWCNTs (0.0034 mg/mL) and acetic acid (0.85 mol/dm³), followed by the addition of NH_4OH solution (0.5 mL). Scale bar = 20 nm.

potential analysis of the complex of a-SWCNT with Cu^{2+} shows a higher stability in alkaline medium than a-SWCNTs (Fig. 6), which could slow down deposition of the composite species to the cathode, resulting in increased growth of the Cu particles on the a-SWCNTs once migrated to the cathode surface.

Since neutralization of the acetic acid solution did not overturn the effects of the complexed copper species on the migration direction of the a-SWCNTs, we investigated the effect of an added complexation agent. The addition of sodium EDTA to the acetic acid solution electrolysis of a-SWCNTs resulted in the partitioning of the a-SWCNTs between both electrodes (Fig. 16). This suggests the addition of EDTA complexes the copper and allows some fraction of the a-SWCNTs to follow their preferred migration route to the anode.
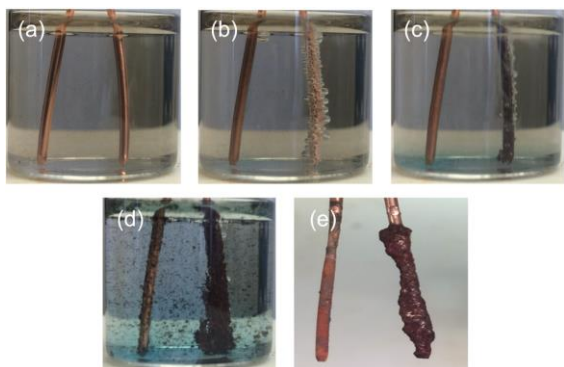

Fig. 16. Partitioning of a-SWCNTs between anode and cathode in experiment involving copper electrodes with a-SWCNTs (0.0034 mg/mL) in an acetic acid solution (0.85 mol/dm³) upon addition of sodium EDTA (0.005 mol/dm³) before and after various time intervals of electrolysis: (a) 0 s, (b) 23 s, (c) 194 s, (d) 885 s, and (e) 1016 s. The left electrode is the anode while the right electrode is the cathode. Snapshots at additional intervals are as shown in Figure S12, while SEM images of related electrodes are shown in Figure S13 in ESI.

EDS analysis of the solid obtained by dispersing a-SWCNTs in $CuSO_4$ solution followed by centrifugation and filtration showed 2.6 at.% Cu. Re-suspending this material in solution and adding EDTA, then centrifugation and filtration showed a Cu content of 0.2 at.%, suggesting a >90% removal of adsorbed copper ions. Presumably the a-SWCNTs that migrated to the anode were the ones with fewer functional groups per SWCNT and hence less Cu to be removed. The reversible nature of the addition of EDTA is also demonstrated from the zeta potential of a-SWCNTs in the presence of Cu^{2+} with the addition of EDTA it is essentially identical to that of a-SWCNTs (see Fig. 6), suggesting that the Cu^{2+} has been removed from the surface of the SWCNTs. Further research evaluating the adsorption/desorption characteristics of SWCNTs in relation to copper species, similar to prior work[37-39] would be useful in optimizing / stabilizing Cu-SWCNT formulations for electrical applications. These would likely involve detailed experimentation related to modifying and activating SWCNT surfaces using a suitable combination of physical and chemical methods.[40] The capability of metal- and graphene oxide species in photocatalytically remediating dye-containing aqueous wastes from the textile industry[41-43] can be coupled

with high surface area nanostructured backbones such as SWCNTs to develop efficient aqueous chemical waste remediation technologies. Such novel materials can also be used in antimicrobial applications.[44] Further, the capability of nanotubes to adsorb metal species can potentially be researched further in relation to remediation of heavy metals from industrial wastes.[45]

Conclusions

While numerous studies have addressed electrophoretic migration of carbon nanotubes in a dispersion, with dispersing agents such as surfactants and polymers,[46-49] this study attempted to address the situations where such dispersing agents were avoided, in order to obtain some foundational insights into the rapidly evolving field metal-nanomaterial composites from an electrochemical perspective. Table 2 below summarizes the observations presented herein.

Table 2. Summary of observations pertaining to reaction conditions described in Table 1.

Sample	Solution composition	Comment
1	Control, without SWCNTs	Aggregate formation at cathode
2	Raw-SWCNTs	Partition between anode and cathode
3	Raw-SWCNTs, $CuSO_4$	Migration to cathode
4	a-SWCNTs	Migration to anode
5	a-SWCNTs, $MeCO_2H$	Migration to cathode
6	a-SWCNTs, $CuSO_4$	Migration to cathode
7	a-SWCNTs, $MeCO_2H$, EDTA	Predominant migration to cathode, with a small migration toward anode

Raw-SWCNTs are highly hydrophobic and could not be dispersed easily and stably in an aqueous electrolytic bath medium; however, with sufficient vortexing it is found that there is a partitioning between anode and cathode resulting from the inhomogeneity of impurities such as catalyst residue. Removal of the catalyst residue through acid treatment (i.e., a-SWCNTs) results in overwhelming migration to the anode. The presence of a small portion that continues to migrate to the cathode suggest that electrolysis could be used as a route to secondary purification of SWCNTs, since the total removal of catalyst residue is important for a number of applications.[28]

The electrolytic migration of SWCNTs to a cathode is promoted by either the presence of catalyst residue or coordinated metals. We, and others, have shown that epoxidized CNTs and graphene are excellent at up-taking metals (in particular hazardous heavy metals) from solution. Unfortunately, in many cases the subsequent separation of the metal-carbon nanomaterial is complex unless a supported system is employed. Electrolysis of the metal-carbon nanomaterial-containing dispersions would result in separation if collection could be facilitated.

Electrode materials also have a bearing on how SWCNTs and/or co-mingled copper (or other metal species) can migrate to electrode surfaces. When both anode and cathode were made of copper, the anode is an active component of the

system. The anode did not get altered when platinum was used.

It was interesting to note the co-migration of a-SWCNTs and copper toward the cathode under an applied electrical field. This migration is likely due to a combination of reasons: (a) adsorption of copper ions onto defect sites of SWCNTs, causing negative surface charges on the nanotube surfaces to be converted to an overall positive charge, and possibly (b) dragging of the a-SWCNTs toward the cathode under the momentum of migration of copper ions.

Oxides of copper were likely present in most copper-based deposits on cathodes, resulting in the deposits possessing a reddish-brown colour. Initial results have shown that use of commercial brighteners helped avoid the brownish colour of the deposit and yield shiny copper-coloured deposits on the cathode likely due to a lower oxygen impurity content.

In this work we have studied the fundamental mechanics underlying the fabrication of Cu-SWCNT composites using a facile direct current electroplating process. In general, heterogeneous composites of copper and SWCNTs were obtained in all cases. The resulting materials have potential as precursor materials for the extrusion of Cu-SWCNT wires with improved high temperature conduction over Cu. Other potential applications of Cu-SWCNT composites can include remediation of dyes found in wastewater generated by the textile industry, adsorption of heavy metals from water, sensors to detect pharmaceutical compounds in the bloodstream, etc. Electrolysis has the ability to allow variation of the relative proportion of added SWCNTs, although subsequent processing of the composite materials though techniques such as compression and extrusion will need to be evaluated.

Conflicts of interest

There are no conflicts to declare.

Acknowledgements

Notes and references

1 P. Jarosz, C. Schauerman, J. Alvarenga, B. Moses, T. Mastrangelo, R. Raffaelle, R. Ridgley, and B. Landi, *Nanoscale,* 2011, **3**, 4542-4553.

2 P. Wilhite, A. A. Vyas, J. Tan, J. Tan, T. Yamada, P. Wang, J. Park, and C. Y. Yang, *Semicond. Sci. Technol.,* 2014, **29**, 054006.

3 C. T. White and T. N. Todorov, *Nature*, 1998, **393**, 240-242.

4 K. Banerjee and N. Srivastava, *Proc. of DAC*, S. Francisco, Ca (USA), Jul 2006, 809-814.

5 O. Hjortstam, P. Isberg, S. Soderholm, and H. Dai, *Appl. Phys. A: Mater. Sci. Process.*, 2004, **78**, 1175-1179.

6 D. F. Lee, M. Burwell, and H. Stillman, *Priority Research Areas to Accelerate the Development of Practical Ultra-conductive Copper Conductors*, Oak Ridge National Laboratory, 2015.

7 C. Subramaniam, T. Yamada, K. Kobashi, A. Sekiguchi, D. N. Futaba, M. Yumura, and K. Hata, *Nat. Commun.*, 2013, **4**, 2202.

8 G. Chai, Y. Sun, J. J. Sun, and Q. Chen, *J. Micromech. Microeng.*, 2008, **18**, 035013.

9 S. Arai, T. Saito, and M. Endo, *J. Electrochem. Soc.* 2010, **157**, D147-D153.

10 S. M. Uddin, T. Mahmud, C. Wolf, C. Glanz, I. Kolaric, C. Volkmer, H. Höller, U. Wienecke, S. Roth, and H.-J. Fecht, *Compos. Sci. Technol.* 2010, **70**, 2253-2257.

11 W. M. Daoush, B. K. Lim, C. B. Mo, D. H. Nam, and S. H. Hong, *Mater. Sci. Eng., A*, 2009, **513–514**, 247–253.

12 K. D. Wright, C. E. Gowenlock, J. C. Bear, and A. R. Barron, *ACS Appl. Mater. Interfaces*, 2017, **9**, 27202-27212.

13 G. Chen, L. Zhang, and J. Wang, *Talanta*, 2004, **64**, 1018-1023.

14 Y. Yang, L. Qu, L. Dai, T.-S. Kang, and M. Durstock, *Adv. Mater.*, 2007, **19**, 1239-1243.

15 Y. Lu, T. Li, X. Zhao, M. Li, Y. Cao, H. Yang, and Y. Y. Duan, *Biomaterials*, 2010, **31**, 5169-5181.

16 W. Lu, H. Song, Y. Jin, H. Zhao, H. Zhao, L. Cao, Z. Li, H. Jiang, and G. Miao, *Physica B*, 2008, **403**, 1793-1796.

17 K. Yamamoto, S. Akita, and Y. Nakayama, *J. Phys. D: Appl. Phys.* 1998, **31**, L34–L36.

18 S. W. Lee, D. S. Lee, H. Y. Yu, E. E. B. Campbell, and Y. W. Park, *Appl. Phys. A*, 2004, *78*, 283-286.

19 W. B. Choi, Y. W. Jin, H. Y. Kim, S. J. Lee, M. J. Yun, J. H. Kang, Y. S. Choi, N. S. Park, N. S. Lee, and J. M. Kim, *Appl. Phys. Lett.* 2001, **78**, 1547-1549.

20 S. H. Kim and M. R. Zachariah, *Nanotechnology*, 2005, **16**, 2149-2152.

21 P. M. Raja, J. Connolley, G. P. Ganesan, L. Ci, P. M. Ajayan, O. Nalamasu, and D. M. Thompson, *Toxicol. Lett.* 2007, **169**, 51-63.

22 M. J. O'Connell, P. Boul, L. M. Ericson, C. Huffman, Y. Wang, E. Haroz, C. Kuper, J. Tour, K. D. Ausman, and R. E. Smalley, *Chem. Phys. Lett.*, 2001, **342**, 265-271.

23 M. J. O'Connell, S. M. Bachilo, C. B. Huffman, V. C. Moore, M. S. Strano, E. H. Haroz, K. L. Rialon, P. J. Boul, W. H. Noon, C. Kittrell, and J. Ma, *Science* 2002, **297**, 593-596.

24 D. Ogrin, J. Chattopadhyay, A. K. Sadana, E. Billups, and A. R. Barron, *J. Am. Chem. Soc.*, 2006, **128**, 11322-11323.

25 K. J. Ziegler, Z. Gu, H. Peng, E. L. Flor, R. H. Hauge, and R. E. Smalley, *J. Am. Chem. Soc.*, 2005, **127**, 1541-1547.

26 D. Lee, P. M. V. Raja, G. L. Esquenazi, and A. R. Barron, *Environ. Sci.: Nano*, 2018, **5**, 103-114.

27 K. D. Wright and A. R. Barron, *C* 2017, **3**, 17.

28 K. S. Zhang, D. Pham, O. Lawal, S. Ghosh, V. S. Gangoli, P. Smalley, K. Kennedy, B. Brinson, W. E. Billups, R. Hauge, W. W. Adams, and A. R. Barron, *ACS Appl. Mater. Interfaces*, 2017, **9**, 37972-37980.

29 K. Jüttner, U. Galla, and H. Schmieder, *Electrochim. Acta*, 2000, **45**, 2575-2594.

30 E. H. Jones, D. A. Reynolds, A. L. Wood, and D. G. Thomas, *Ground Water*, 2011, **49**, 172-183.

31 O. Moradi, K. Zare, and M. Yari, *Int. J. Nano Dim.*, 2011, **1**, 203-220.

32 P. N. Alagappan, J. Heimann, L. Morrow, E. Andreoli, and A. R. Barron, *Sci. Reports*, 2017, **7**, 6682.
33 M. Devaraj, R. Saravanan, R. Deivasigamani, V. K. Gupta, F. Gracia, and S. Jayadevan, *J. Mol. Liquid.*, 2016, **221**, 930-941.
34 S. Niyogi, M. A. Hamon, H. Hu, B. Zhao, P. Bhowmik, R. Sen, M. E. Itkis, and R. C. Haddon, *Acc. Chem. Res.*, 2002, **35**, 1105-1113.
35 T. W. Ebbesen, H. Hiura, M. E. Bisher, M. M. J. Treacy, J. L. Shreeve-Keyer, and R. C. Haushalter, *Adv. Mater.*, 1996, **8**, 155-157.
36 H. Hu, A. Yu, E. Kim, B. Zhao, M. E. Itkis, E. Bekyarova, and R. C. Haddon, *J. Chem. Phys. B*, 2005, **109**, 11520-11524.
37 A. Mittal, J. Mittal, A. Malviya, and V. K. Gupta, *J. Colloid Interface Sci*., 2010, **344**, 497-507.
38 N. Mohammadi, H. Khani, V. K. Gupta, E. Amereh, and S. Agarwal, *J. Colloid Interface Sci.*, 2011, **362**, 457-462.
39 T. A. Saleh and V. K. Gupta, *J. Colloid Interface Sci.*, 2012, **371**, 101-106.
40 T. A. Saleh and V. K. Gupta, *Advances in colloid and interface science*, 2014, **211**, 93-101.
41 T. A. Saleh and V. K. Gupta, *J. Colloid Interface Sci*., 2011, **362**, 337-344.

42 R. Saravanan, S. Karthikeyan, V. K. Gupta, G. Sekaran, V. Narayanan, and A. Stephen, *Materials Science and Engineering: C*, 2013, **33**, 91-98.
43 D. Robati, B. Mirza, M. Rajabi, O. Moradi, I. Tyagi, S. Agarwal, and V. K. Gupta, *Chemical Engineering Journal*, 2016, **284**, 687-697.
44 R. Saravanan, M. M. Khan, V. K. Gupta, E. Mosquera, F. Gracia, V. Narayanan, and A. Stephen, *RSC Adv.*, 2015, **5**, 34645-34651.
45 V. K. Gupta, A. Nayak, and S. Agarwal, *Environmental Engineering Research*, 2015, **20**, 1-18.
46 K. Yamamoto, S. Akita, and Y. Nakayama, *J. Phys. D: Appl. Phys.*, 1998, **31**, L34-L36.
47 W. B. Choi, Y. W. Jin, H. Y. Kim, S. J. Lee, M. J. Yun, J. H. Kang, Y. S. Choi, N. S. Park, N. S. Lee, and J. M. Kim, *Appl. Phys. Lett.*, 2001, **78**, 1547-1549.
48 S. W. Lee, D. S. Lee, H. Y. Yu, E. E. B. Campbell, and Y. W. Park, *Appl. Phys. A*, 2004, **78**, 283-286.
49 Y. Lu, T. Li, X. Zhao, M. Li, Y. Cao, H. Yang, and Y. Y. Duan, *Biomaterials*, 2010, **31**, 5169-5181.